Observational Constraints on the Cloud Thermodynamic Phase in Midlatitude Storms

CATHERINE M. NAUD

Department of Applied Physics and Applied Mathematics, Columbia University, and NASA Goddard Institute for Space Studies, New York, New York

ANTHONY D. DEL GENIO

NASA Goddard Institute for Space Studies, New York, New York

MIKE BAUER

SGT Inc., NASA Goddard Institute for Space Studies, New York, New York

(Manuscript received 4 October 2005, in final form 3 February 2006)

ABSTRACT

The conditions under which supercooled liquid water gradually gives way to ice in the mixed-phase regions of clouds are still poorly understood and may be an important source of cloud feedback uncertainty in general circulation model projections of long-term climate change. Two winters of cloud phase discrimination, cloud-top temperature, sea surface temperature, and precipitation from several satellite datasets (the NASA *Terra* and *Aqua* Moderate Resolution Imaging Spectroradiometer, and the Tropical Rainfall Measuring Mission) for the North Atlantic and Pacific Ocean basins are analyzed to better understand these processes. Reanalysis surface pressures and vertical velocities are used in combination with a synoptic storm-tracking algorithm to define storm tracks, create composite storm dynamical and cloud patterns, and examine changes in storm characteristics over their life cycles. Characteristically different storm cloud patterns exist in the Atlantic and Pacific and on the west and east sides of each ocean basin. This appears to be related to the different spatial patterns of sea surface temperature in the two ocean basins. Glaciation occurs at very warm temperatures in the high, thick, heavily precipitating clouds typical of frontal ascent regions, except where vertical velocities are strongest, similar to previous field experiments. Outside frontal regions, however, where clouds are shallower, supercooled water exists at lower cloud-top temperatures. This analysis is the first large-scale assessment of cloud phase and its relation to dynamics on climatologically representative time scales. It provides a potentially powerful benchmark for the design and evaluation of mixed-phase process parameterizations in general circulation models and suggests that assumptions made in some existing models may negatively bias their cloud feedback estimates.

1. Introduction

Cloud feedbacks are still the major uncertainty for predicting climate sensitivity to external perturbations, in part due to the absence of observational constraints suitable for distinguishing different parameterizations in general circulation models (GCMs). One such outstanding problem concerns the conditions under which cloud exists in the ice versus the liquid phase. Early prognostic cloud water parameterizations for stratiform clouds resulted in significantly lower climate sensitivities to a doubling of CO_2 than previous diagnostic schemes (Mitchell et al. 1989; Senior and Mitchell 1993), one reason being a cloud phase feedback. The relative occurrence of the liquid phase should increase as temperature rises, and, given the different microphysical and radiative properties of ice and liquid clouds, changes in cloud fraction, water content, and reflectivity will result. The feedback depends, however, on the temperature range over which the liquid–ice transition occurs, which determines the relative importance of competing longwave and shortwave contributions to the feedback (Li and Le Treut 1992).

Available observations from field experiments give different impressions of the persistence of supercooled liquid water at cold temperatures. Aircraft data compiled in a variety of midlevel clouds over the former Soviet Union by Feigelson (1978) suggest that super-

Corresponding author address: Catherine Naud, NASA GISS, 2880 Broadway, New York, NY 10025.
E-mail: cnaud@giss.nasa.gov

cooled water exists down to a temperature of −40°C. On the other hand, Bower et al. (1996), in a study similar to that previously conducted by Moss and Johnson (1994), found mostly ice at temperatures below −15°C in primarily thick frontal clouds in the vicinity of the British Isles, while convective clouds in several locations exhibited supercooled water down to colder temperatures. Using ground-based lidar measurements, Hogan et al. (2003a,b) confirmed the existence of a layer of supercooled droplets at cloud top down to temperatures as cold as −30°C for two midlatitude continental locations.

GCMs have used these conflicting results to make various choices about the parameterization of cloud phase in stratiform clouds. Many models specify the ice fraction of condensate solely as a function of temperature, some assuming all ice at temperatures <-15°C (Le Treut and Li 1991; Senior and Mitchell 1993; Hasumi and Emori 2004) and others allowing supercooled water down to −30° (Kiehl et al. 1998) or −40°C (Boville et al. 2006). Others modify an initial phase–temperature relationship in the presence of diagnosed microphysical processes (Del Genio et al. 1996). The most sophisticated schemes carry separate liquid and ice prognostic variables and parameterize microphysical processes to determine phase interactively. The choices in these schemes that affect cloud phase have been made by comparing to the Bower et al. (1996) frontal cloud observations (Rotstayn et al. 2000), to isolated case studies (Wilson and Ballard 1999), or to parameters other than cloud phase (Lohmann and Roeckner 1996).

More recently, satellite data have been used to retrieve cloud phase information. Doutriaux-Boucher and Quaas (2004) used polarimetric satellite data to evaluate a global lower limit of −32°C for 100% ice fraction but they did not consider geographic or temporal variations of this quantity, although, using the same polarimetric data, Giraud et al. (2001) previously found differences between ocean and land for temperatures of full glaciation. A 10.5-h spaceborne lidar dataset gave some insights into the global distribution of supercooled droplets at cloud top, and frequent occurrences were found in Southern Hemisphere weather systems (Hogan et al. 2004).

The field experiments show considerable scatter in ice fraction at any temperature, indicating the importance of microphysical and dynamical processes. Aside from temperature, glaciation may also be a function of the vigor of vertical motions and precipitation, depth and age of the cloud, and concentration of ice nuclei. Disagreements among the measurements quoted above may simply reflect sampling of different types of clouds in different locations and dynamic or microphysical conditions. Satellite observations have the potential to reconcile the disparate field experiment results while providing a climatologically significant sample suitable for designing and evaluating more physically based parameterizations of cloud phase.

In this paper we investigate how atmospheric dynamics and environmental conditions affect the temperature dependence of the cloud phase transition by using satellite-derived estimates of cloud-top temperature and phase discrimination. We focus on the oceanic midlatitude storm tracks since these are locations of primarily stratiform clouds that exhibit considerable variation in cloud-top temperature and phase. (Tropical stratiform anvils and cirrus clouds are almost exclusively ice at cloud top, while polar clouds, which exhibit important mixed-phase variability, are more difficult to diagnose from satellites.) Cloud-top temperature and phase retrieved with the Moderate Resolution Imaging Spectroradiometer (MODIS; Salomonson et al. 1989) on board the NASA satellites *Terra* (launched in December 1999) and *Aqua* (launched in March 2002) are collected over the North Atlantic and Pacific during winter months (December, January, and February), from December 2002 to February 2004. A storm-tracking technique is applied to the National Centers for Environmental Prediction–National Center for Atmospheric Research (NCEP–NCAR) reanalysis surface pressures in order to isolate the extratropical storm-track preferred paths. The MODIS cloud-top temperature and phase relationship and its variation along the paths of midlatitude storms is examined by dividing each ocean basin into west and east regions. Composites of cloud and environmental properties centered on a storm pressure minimum (cf. Lau and Crane 1995; Klein and Jakob 1999; Bauer and Del Genio 2006) are used to understand how MODIS cloud-top properties vary around a storm pressure center in the western and eastern portion of the storm track areas and between the Atlantic and Pacific Oceans.

Section 2 describes the various datasets used in this study as well as the methods for data extraction. Section 3 presents the results, section 4 is a discussion of the implications of our work, and section 5 contains the conclusions of this study.

2. Data and methods

a. Extratropical storm tracks and associated precipitation

Bauer and Del Genio (2006) used NCEP–NCAR reanalysis (Kalnay et al. 1996; Kistler et al. 2001) surface pressures to detect extratropical synoptic storms. For

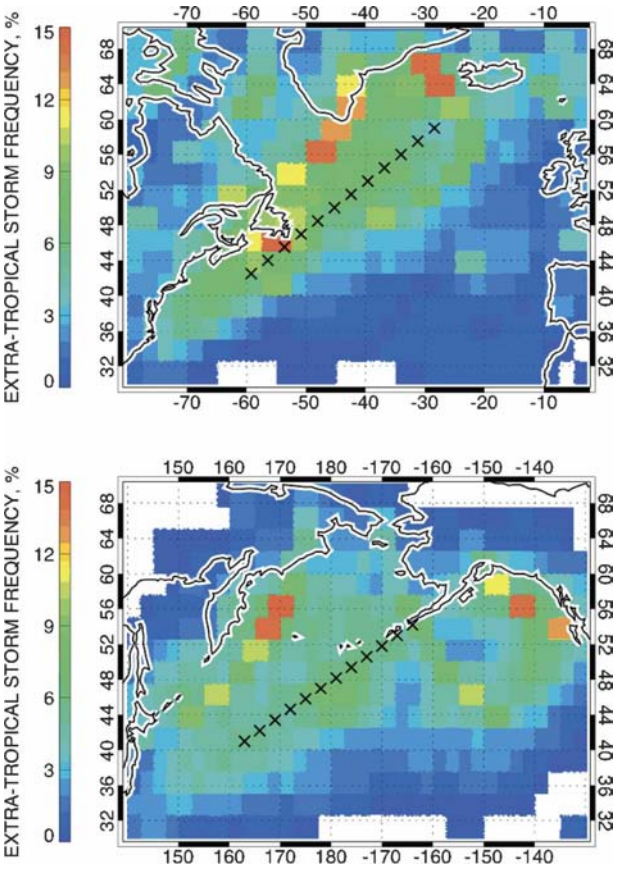

FIG. 1. Extratropical storm frequency of occurrence over time (%), for the period December 2002–February 2004 over the (top) North Atlantic Ocean and (bottom) North Pacific Ocean.

the two winters (December, January, and February) from December 2002 to February 2004, for which all datasets that we use overlap, their algorithm produces a list of all storms that occurred in the Northern Hemisphere midlatitude regions (30°–70°N), giving for each 6-h step of their lifetime their location and central pressure. In addition, vertical velocities in a ± 25° latitude–longitude area centered on the surface pressure minimum are extracted from the reanalysis.

Storm frequency maps are obtained by accumulating them into an equal area grid and then reprojecting onto a 2° × 2.5° latitude–longitude grid. The resulting storm frequency of occurrence for the winters from December 2002 to February 2004 is derived separately for the Atlantic (80°E–0°) and Pacific (140°E–130°W) Ocean basins (Fig. 1). The frequency maxima give the general location and direction of the storm tracks for the two winters selected here. It can be observed in these figures that, while storms are confined to a well-defined area over the Atlantic, they are more spread out over the Pacific, and it is more difficult to define the average trajectory of the storm tracks in this basin. This variability may be due to shifts of the Pacific storm track during extreme El Niño–La Niña phases (Eichler and Higgins 2006; Orlanski 2005). To refine the idealized trajectory, we use the Goddard Institute for Space Studies (GISS) storm atlas (Chandler and Jonas 1999), which uses a similar tracking technique over a longer time period (2000–04), and visually estimate the storm trajectories for both oceans, as marked with the crosses in Fig. 1.

For each storm in the database for both winters, each 6-h time step in a storm's lifetime is considered independently, and four geographical subsets are constructed according to the location of the pressure minimum at each step. These subsets are west Atlantic (30°–60°N, 75°–50°W), east Atlantic (30°–60°N, 50°W–0°), west Pacific (30°–60°N, 150°E–177.5°W) and east Pacific (30°–60°N, 177.5°–135°W). There are 48 distinct storms and 252 total time steps for the west Atlantic, 42 storms and 278 steps for the east Atlantic, 62 storms and 317 steps for the west Pacific, and finally 52 storms and 334 steps for the east Pacific.

Precipitation rates are obtained from an experimental 3-hourly Tropical Rainfall Measuring Mission (TRMM) combined microwave–infrared dataset (Huffman et al. 2003) for the 6 months selected here. These rates are available globally up to 60° latitude, so storms with a low pressure center beyond 60°N were ignored in this study. They are composited for each subregion defined above using each pressure minimum as the center of a ±25° latitude–longitude grid of 1° × 1° cells and accumulating the collocated and coincident precipitation rates in each cell. This gives the spatial distribution of precipitation in the area affected, for each time step, by a typical storm for each subregion. These precipitation rates are used as qualitative indicators of the presence of vertically extended clouds and indirectly indicate areas where glaciation processes may be occurring. They are also a means of verifying the validity of the reanalysis vertical velocity fields (i.e., strong precipitation and 500-mb ascent should generally coincide if both products contain real information content).

b. Cloud properties from MODIS

MODIS measures radiances in 36 spectral bands from 0.4 to 14.2 μm with a nadir spatial resolution from 250 m to 1 km depending on the spectral band. The MODIS cloud products are generated on a 5-min granule basis of 2030 along-track and 1350 across-track 1-km resolution pixels. MODIS data have been reprocessed four times from the beginning of the mission following improvements in the data processing algorithms, and collection-4 cloud products were used in

this study. Cloud product generation is fully described in Platnick et al. (2003) and King et al. (2003), so only a brief description of cloud-top temperature and phase retrievals is provided here.

MODIS cloud-top pressures are first calculated operationally using the CO_2-slicing technique (Menzel et al. 2002). Due to signal-to-noise issues, CO_2-slicing cloud-top pressures are generally limited to the range from approximately 700 hPa (i.e., about 3 km above sea level) up to the tropopause. When low clouds are present, the MODIS algorithms defer to the infrared window technique where cloud-top pressure and temperature are determined through comparison of model-calculated and observed 11-μm radiances. Cloud-top pressures are first obtained at 5-km resolution using averaged 1-km radiances. They are then converted into equivalent cloud-top temperatures with a gridded meteorological product provided every 6 h by the NCEP Global Data Assimilation System (GDAS: Derber et al. 1991). MODIS cloud-top pressure accuracy was assessed against airborne lidar (Frey et al. 1999), ground-based radar and lidar (Naud et al. 2002, 2004; Mace et al. 2005), and other passive and active satellite instruments (Naud et al. 2005a,b). These studies reveal that the accuracy of cloud-top boundaries is within 1 km when clouds are single layered and have sufficient optical depth. Naud et al. (2005b) show that optical depths less than 0.3 cause a greater error in cloud-top height retrievals, even more so for multilayer cloud situations. This may cause high and thin ice clouds to be missed if a lower water cloud is present.

Cloud-top phase is estimated from a series of tests involving both visible and near-infrared reflectances and infrared brightness temperatures [see Platnick et al. (2003) for a complete description of the algorithm]. A decision tree provides cloud composition at 1-km resolution pixel level, indicating if a pixel is mainly composed of ice or liquid water. This decision tree involves cloud mask tests (using 1.38-, 3.7-, and 11-μm channels), differences in optical constants between liquid and ice in the infrared (8 and 11 μm) and shortwave infrared (1.6 and 2.1 μm), and finally the cloud-top temperature information. The thresholds are adapted to the different possible surface types (e.g., ocean, land, etc.). Any pixel that is not flagged as liquid or ice is discarded. This problem was found to be a rare occurrence (e.g., less than 1% of all pixels per granule). Because of the use of visible and near-infrared channels, this product is only available in daylight areas so nighttime pixels or granules are discarded. To match the 1-km resolution of cloud phase with the 5-km resolution cloud-top temperatures, the phase of the central pixel in 5×5 pixel subsets is used. An alternative technique was tested using the median phase in the same 5×5 pixel subsets instead. One hundred MODIS *Aqua* granules were randomly selected and, for forty 2-K temperature bins, the ice cloud fraction was derived as the ratio of the number of pixels with ice phase to the number of pixels with ice or water phase. The difference between ice fractions obtained with the central pixel and median phase was calculated as a function of temperature. The largest difference was found to be 0.04 at 255 K, and adding more MODIS data was found to decrease this value. For the larger number of granules used when adding *Aqua* and *Terra* the error introduced in the ice cloud fraction by the central pixel selection is less than 0.02. The central pixel procedure is used by the MODIS team to convert the 1-km cloud mask into the 5-km cloud mask, so this mode of selection is used here.

No formal accuracy assessment of the phase retrievals had been conducted at the time of this study, mainly because independent and coincident phase information is difficult to obtain. It is thus difficult to assess the weaknesses of the retrieval technique, but we can speculate that thin ice cloud over low water cloud situations will cause errors, as will mixed-phase clouds when both liquid and ice phases are present. An independent comparison between MODIS cloud-top temperatures and coincident cloud radar-derived cloud-top temperatures at the Department of Energy (DOE) Atmospheric Radiation Measurement Program Southern Great Plains site (Fig. 2) reveals that most of the disagreement occurs for high-level cloud situations where MODIS cloud-top temperatures are warmer than the radar cloud-top temperature. For these outlier cases, the MODIS phase retrieval indicates water, suggesting that the cloud-top temperature and phase retrieval algorithms have similar weaknesses in multilayer cloud situations, both detecting the lower rather than the higher cloud. This exercise does not allow us to evaluate an absolute error for the relationship between cloud phase and temperature with MODIS, but, since the errors in each tend to be correlated, we anticipate that the uncertainty in the phase–temperature relationship is less than the error in either parameter separately; that is, even if both retrievals fail to refer to the highest cloud in the scene, they are referring to the same cloud. Previous MODIS cloud-top height assessments (Naud et al. 2005a) showed that errors found at the Southern Great Plains site were consistent with errors found at Chilbolton, United Kingdom, situated in the eastern portion of the Atlantic storm track.

MODIS cloud properties are assigned to cloud top as they are retrieved with a downward-looking passive sensor. Consequently, this instrument does not offer in-

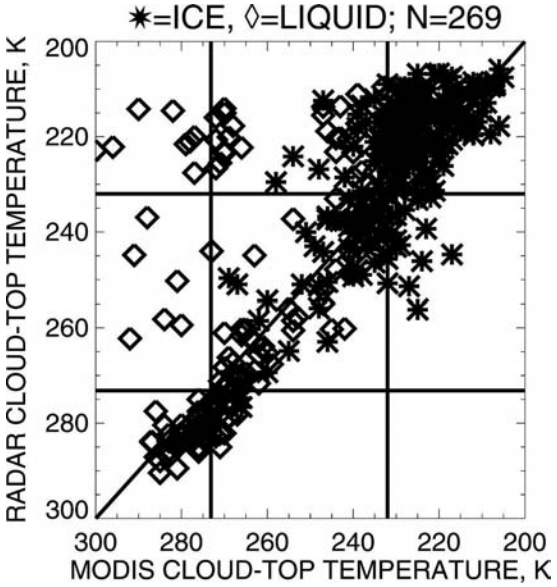

FIG. 2. Radar cloud-top temperature vs MODIS cloud-top temperature, for ice (*) and liquid (◊) MODIS phase retrievals. The radar cloud-top temperature data were collected between 2000 and 2003 at the ARM SGP site and converted from cloud-top heights using ECMWF profiles. The radar time series were sampled during the 5-min of coincident MODIS overpass and the median cloud-top height was used for the comparison with the median MODIS cloud-top temperature obtained in a ±0.2° latitude–longitude box centered on the SGP site. The MODIS phase information was chosen to be the modal value within the same latitude–longitude box. The total number of cases was 269.

formation on properties within the clouds, and all the results presented hereafter pertain to cloud-top properties. Nonetheless, we will show later that cloud phase statistics near cloud top, and their variation with the synoptic situation, are not markedly different from those acquired by aircraft in cloud interiors.

In addition, each MODIS cloud product granule contains a 5 km × 5 km resolution sea surface temperature (SST) array that is interpolated from the 1° × 1° weekly NOAA Optimum Interpolation SST dataset (Reynolds and Smith 1994); this product is also used here. These temperatures were obtained in cloud-free situations.

Figure 3 illustrates the MODIS cloud phase retrieval and associated fields for an east Atlantic synoptic storm observed on 19 January 2003, about 30 h after it was first detected in the reanalysis. Ice is present exclusively at cloud top in the comma-shaped high cloud shield east and north of the surface low in advance of the surface front, but elsewhere liquid water exists at cloud top at various temperatures in different parts of the storm system. 1) In the 500-mb frontal ascent and precipitation region just east and south of the low, both cloud-top temperature and phase are highly variable on small scales, while cold (<250 K) liquid water cloud tops occur just west of the low in weak ascent; 2) along the upward-sloping frontal surface a narrow band of supercooled water exists along the edge of the ice-only high cloud shield; 3) Nonprecipitating midlevel water clouds (altostratus or altocumulus) in the 500-mb descent region west of the low (behind the cold front) are much colder (<260 K) than the low-level liquid water clouds in other descent areas east and north of the front.

c. Data extraction methods

MODIS 5-min granules obtained from both NASA *Terra* (equator-crossing local time 1030) and *Aqua* (equator-crossing local time 1330) platforms are collected over the North Pacific (30°–65°N, 150°E–135°W) and North Atlantic (30°–65°N, 75°W–0°) oceans for all winter months (December, January, and February) from December 2002 to February 2004.

The cloud properties are extracted in the following manner: 1) cloud-top temperatures are divided into 2-K bins from 210 to 290 K; 2) the number of MODIS 5 km × 5 km water or ice cloud pixels that fall into a cell of a 2° × 2.5° global grid is estimated for each cloud-top temperature interval; 3) the number of MODIS 5 km × 5 km ice-cloud-only pixels that fall into a cell of the 2° × 2.5° global grid is estimated for each cloud-top temperature interval. For each 2° × 2.5° grid cell, the ice cloud fraction per temperature bin is estimated by dividing the number of ice pixels by the number of ice and water pixels. This is only calculated once all MODIS granules for both winters have been accumulated. In addition, the cloud-top temperature for exactly 50% ice fraction (T_{50}) is estimated per grid cell by interpolating the relationship obtained for all temperature bins between ice cloud fraction and cloud-top temperature aggregated over both winters. Consequently, there is a unique value of T_{50} per grid cell. This diagnostic does not imply that phase is only a function of temperature; as we show below; it merely provides a simple way to characterize the statistics of time-mean geographic and synoptic-scale variations in mixed-phase behavior.

Ice fraction at a given temperature is highly variable in time, of course, as field experiments have made clear. Figure 4 illustrates this dynamical variability. It shows the instantaneous ice fraction per temperature bin for MODIS passes over two grid cells over the Atlantic during a particular 14-day period (comparable to the length of a typical field experiment) and its relation to the long-term diagnostic T_{50}. Each point shows the ice fraction per temperature bin evaluated for each selected MODIS granule when a temperature bin was populated by at least 10 pixels (otherwise no ice fraction was available for this temperature bin and the

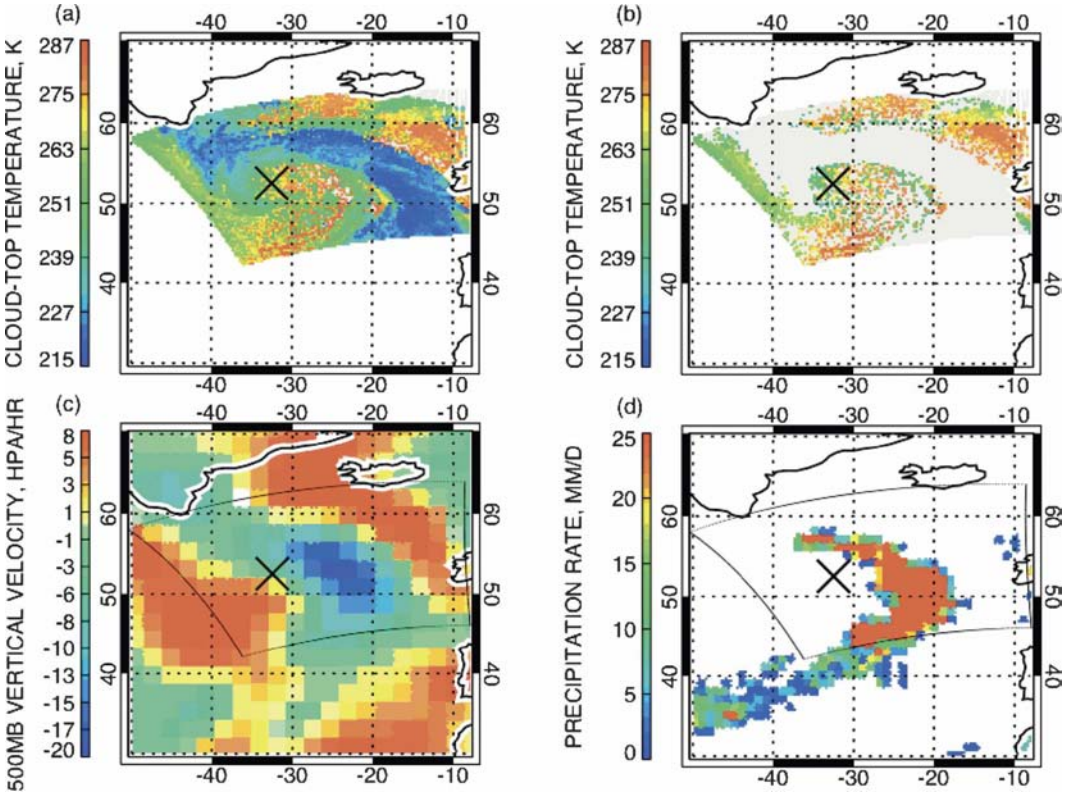

FIG. 3. Storm on 19 Jan 2003 over the Atlantic Ocean; (a) 1200 UTC, *Aqua* overpass at 1430 UTC, MODIS cloud-top temperature; (b) as in (a), but only for liquid water clouds; (c) 500-mb vertical velocity at 1200 UTC, and (d) TRMM precipitation rate at 1200 UTC.

point is not plotted). Despite the scatter, systematic differences in ice phase occurrence between the two locations can be seen: The higher-latitude cell, poleward of the climatological storm track, is dominated by liquid at warmer temperatures and transitions systematically to mostly ice at colder temperatures. The lower-latitude cell, at a location that experiences frequent frontal passage, has greater scatter and a general preference for ice at all but the warmest subfreezing temperatures.

The solid lines on each figure represent the total ice fraction, once all pixels available in these grid cells were accumulated in each temperature bin for both *Aqua* and *Terra* and both winters. The temperature obtained from the intersect between the solid line and 0.5 ice fraction is T_{50} (the dashed vertical line) for these grid cells. The ~10-K difference in T_{50} between the two locations conveniently summarizes the general tendency for liquid to persist to colder temperatures in the higher-latitude grid cell.

The same method is applied to obtain T_{50} in the ±25° grid centered on each storm pressure minimum for the four subregions defined in section 2a, where ice cloud fraction is obtained after accumulating all of the MODIS pixels that are found overlapping a storm area within 3 h. In addition, similar composites are created for the median cloud-top temperature (regardless of the cloud phase) and SST.

3. Results

a. *Change in temperature of glaciation across Atlantic and Pacific Oceans*

The evolution of the relationship between ice cloud fraction and cloud-top temperature as synoptic storms travel eastward across both ocean basins is first tested by using a rough estimate of the general propagation direction of storms. We select all 2° × 2.5° grid cells within 2° latitude–longitude of the visually estimated storm tracks (defined by 12 latitude–longitude points along the tracks in Fig. 1) and equally divide them into two regions (west and east, six points each). The ice cloud fraction as a function of cloud-top temperature is then calculated for each region and each ocean (Fig. 5). Over the Atlantic (black lines), ice forms at warmer temperatures as the storms move eastward; that is, T_{50} increases by ~7 K from west (solid line) to east (dashed line). Over the Pacific (red lines), as the storms move

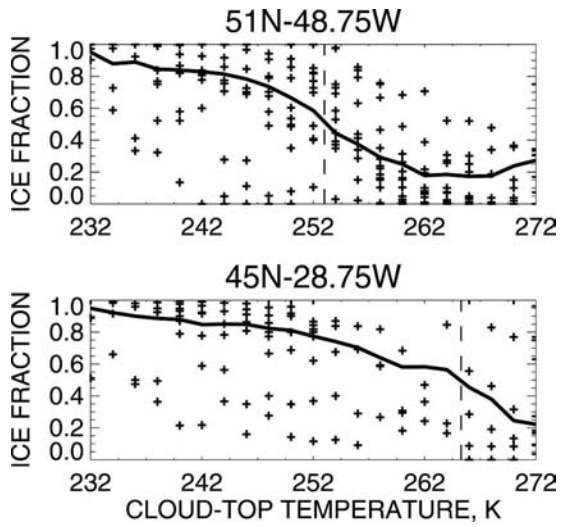

FIG. 4. Ice cloud fraction as a function of cloud-top temperature (+) calculated per MODIS 5-min granule that encompasses grid cells (51°N, 48.75°W) and (45°N, 28.75°W). Twenty MODIS *Aqua* granules over 14 days were selected for each grid cell for which at least 100 pixels were found in the grid box. Ice fractions are kept and plotted if at least 10 pixels populated a temperature bin. The solid line represents ice cloud fractions calculated once all MODIS *Terra* and *Aqua* over both winters are accumulated in each temperature bin and grid cell. The dashed line shows the T_{50} value obtained from the intersection of the solid line with 50% ice.

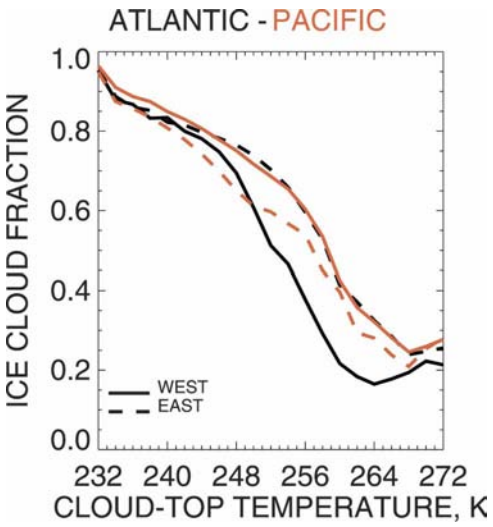

FIG. 5. Ice cloud fraction (number of ice clouds detected divided by number of ice and water clouds detected per 2-K temperature bins) as a function of cloud-top temperature from MODIS, sampled along ideal storm trajectories divided into two regions: west (solid) and east (dashed) over the Atlantic basin (black) and Pacific basin (red), for the period December 2002–February 2004.

eastward, T_{50} instead slightly decreases (~2 K), but this is more obvious for the lower temperature range, that is, for cloud-top temperatures less than 255 K. Thus, along the chosen storm paths, either the impact of dynamics or environmental factors on glaciation is different over the Atlantic and Pacific. We verified that these differences still held when reproducing Fig. 5 for each winter separately.

Figure 6 shows the interpolated MODIS T_{50} for the Atlantic and Pacific Oceans. These cloud-top temperature maps are smoothed by using a 3×3 pixels moving subset and assigning the corresponding median cloud-top temperature to the central pixel. Figure 6 reveals a west–east increase in T_{50} over the Atlantic, with ice formation at consistently warmer temperatures south and east of the storm track, in the expected warm sector and warm front regions. Over the Pacific, however, T_{50} increases primarily from north to south and is less tightly coupled to the mean storm track orientation.

These observations suggest differences between the two oceans, possibly in the storm tracks themselves. Indeed, the two storm tracks are known to exhibit other differences, for example, the longer, stronger, more zonal Asian jet cyclogenesis region for the Pacific track (Bauer and Del Genio 2006), the greater interannual variability of the Pacific track (Eichler and Higgins 2006; Orlanski 2005), the more frequent seeding of the Atlantic storm track by Pacific disturbances than vice versa (Hakim 2003), and the midwinter suppression of baroclinic wave activity only over the Pacific (Nakamura 1992; Chang et al. 2002; Deng and Mak 2005). We tested whether this latter feature could explain some of the differences observed in Figs. 5 and 6 by extracting December, January, and February data separately for the two winters. There was no noticeable difference in ice fraction as a function of temperature over the Pacific from one month to the next, or when comparing west and east.

The more important feature appears to be the different SST distributions in the two oceans: The temperature gradient is oriented approximately north–south over the Pacific but more northwest–southeast over the Atlantic (Fig. 7). The T_{50} maps reflect these tendencies. The relationship between ice fraction and cloud-top temperature changes when we shift the location of the ideal storm track within the observed range of variability, so it is possible that the different behavior of T_{50} observed over the Atlantic and Pacific in Fig. 5 (the temperature for which the curves intersect with the 0.5 horizontal axis) is an artifact of the choice of preferred storm path. To unambiguously compare the two ocean basins and the two sides of each storm track, we instead examine composites of cloud properties centered on the storm pressure minima for all locations both on and off the nominal tracks.

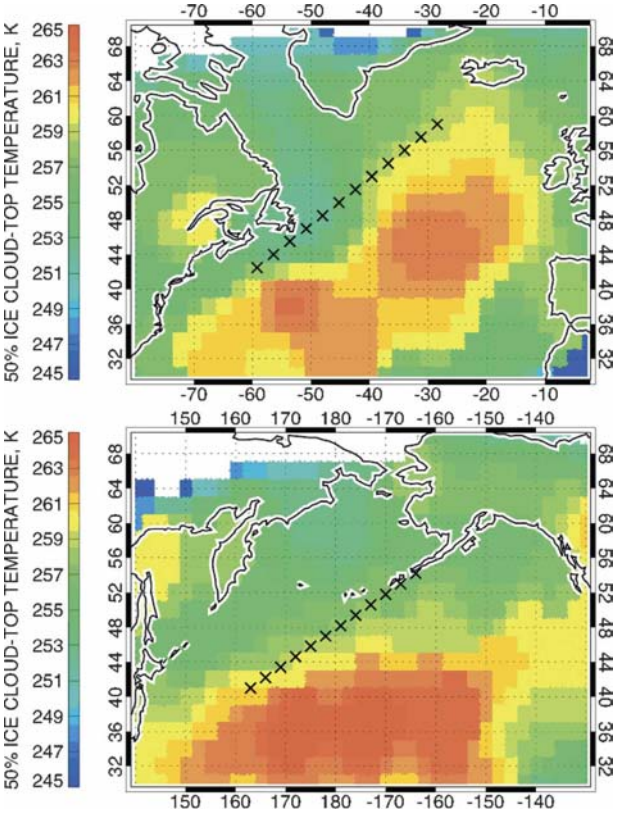

FIG. 6. MODIS T_{50} distribution for the (top) North Atlantic Ocean and (bottom) North Pacific Ocean from December 2002 to February 2004. The crosses indicate the general direction of the storm tracks. Areas with no phase retrievals (mainly because of the lack of daylight) are shown in white.

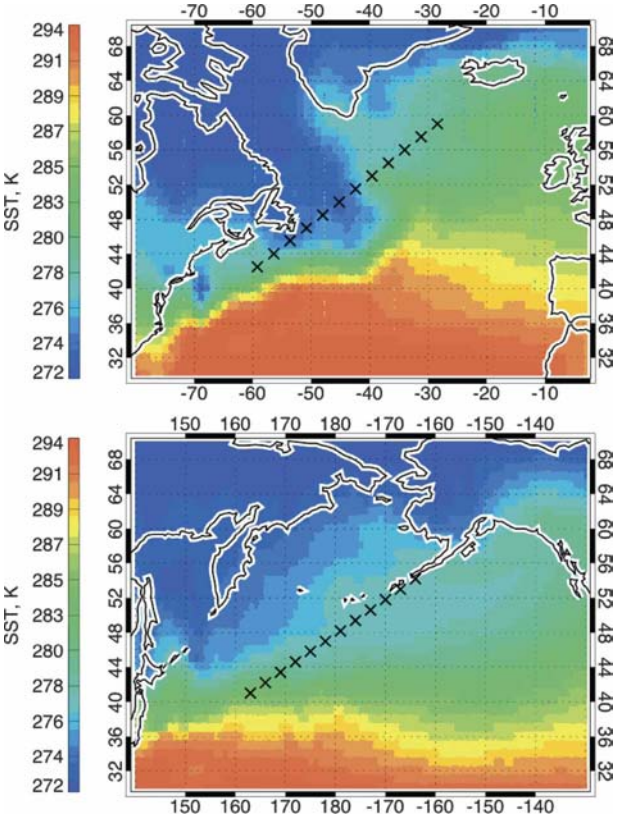

FIG. 7. NOAA Reynolds sea surface temperature for the (top) North Atlantic Ocean and (bottom) North Pacific Ocean averaged over December 2002–February 2004. The crosses indicate the general direction of the storm tracks.

b. Composites of cloud and surface properties centered on storm surface pressure minima

Synoptic storm composites of 500-hPa pressure vertical velocity for the west and east regions of the Atlantic and Pacific are shown in Fig. 8. The composite patterns retain the classic comma structure of baroclinic storms seen in the single-case example of Fig. 3 with peak ascent just north and east of the surface low (indicated by the +), a broad (caused by the displacement from one storm and time step to another) region of ascent east of the low marking the warm front, a second region of ascent extending south and west where the warm sector and cold front occur, and strong descent behind the cold front west of the surface low. In both ocean basins the typical storm is more intense in the western cyclogenesis regions and weakens to the east, more so for Pacific than Atlantic storms. The warm sector–cold front region is broader and extends farther west for Pacific storms than Atlantic storms.

Composites of TRMM precipitation (Fig. 9) generally follow the vertical velocity pattern, with cold front precipitation extending ~20° farther west of the surface low in the Pacific than the Atlantic. This feature has also been reported by Chang and Song (2005). The one departure from the vertical velocity behavior is that Pacific rainfall in the warm sector decreases less rapidly from west to east than Atlantic rainfall.

The composite SST fields experienced by synoptic storms (Fig. 10) are noticeably different for the two ocean basins. In both the Atlantic and Pacific there is a general northwest–southeast SST gradient, maximum near the surface low, and decreasing eastward across both oceans. This is consistent with the general orientation of the storm tracks and the classical understanding of peak cyclogenesis in locations of peak baroclinicity. However, the SST isotherms are more zonal in the Pacific basin. Thus, the different vertical velocity and precipitation composite patterns for the two ocean basins, and specifically the greater westward extent of cold front ascent and precipitation for the Pacific, may be associated with the warmer waters that Pacific storms typically encounter southwest of the surface low.

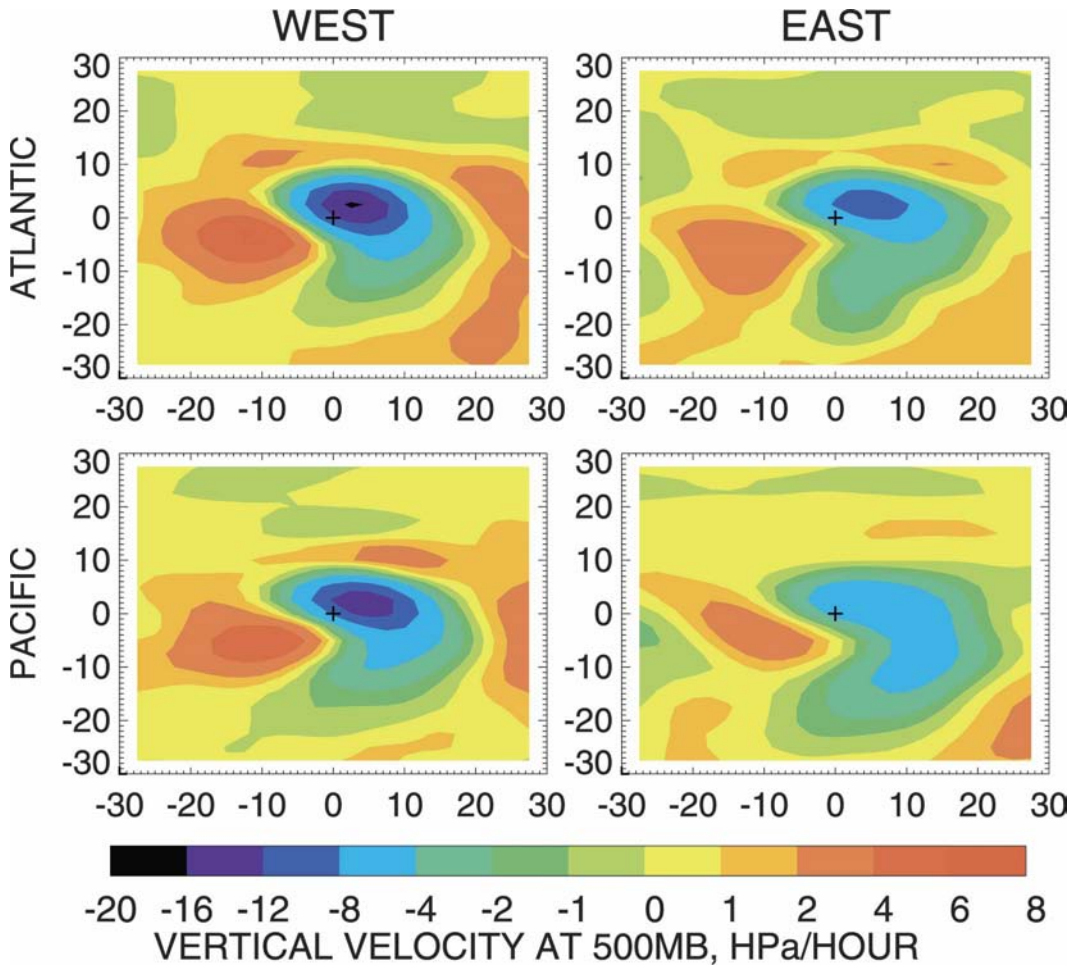

FIG. 8. Composites of 500-hPa pressure vertical velocity (negative upward) obtained from the NCEP–NCAR reanalysis for all storm time steps, over the Atlantic Ocean (top left) west and (top right) east of 50°W and the Pacific Ocean (bottom left) west and (bottom right) east of 177.5°W, for all winter months from December 2002 to February 2004. The + indicates the sea level pressure minimum.

Figure 11 shows the storm composite structure of the T_{50} field. The warmest T_{50} in each subregion is generally in areas of ascent and heavy precipitation, and a more zonally oriented pattern of the warmest T_{50} values occurs in the Pacific than in the Atlantic. In these frontal regions $T_{50} \approx 260$–265 K, indicating that on average liquid water is restricted to warmer temperatures than in other parts of the storm. Our results at cloud top are similar to observations at various cloud levels by Bower et al. (1996) in similar synoptic situations. Elsewhere, though, supercooled liquid survives to much colder temperatures, with $T_{50} \approx 250$–255 K. These parts of the storm are generally nonconvective and consist of shallower nonprecipitating clouds often observed to be liquid at cloud top (Rauber and Tokay 1991; Hogan et al. 2004).

Although warm T_{50} occurs primarily in frontal ascent zones, this association does not directly explain geographic variations in T_{50}. Vertical velocity, precipitation, and SST gradient all decrease from west to east in the frontal regions in both ocean basins (Figs. 8–10), but ice formation occurs at warmer temperatures moving west to east instead. (This behavior is consistent with the Atlantic storm track differences in Fig. 5 but not the Pacific differences, suggesting that the Pacific storm track used in that figure may not be representative of the full population of storms that occur both on and off the nominal track.) We discuss how these geographic differences in storm strength may lead to the observed eastward increase in T_{50} in the next section.

4. Discussion

Other than storm intensity, several other factors that can vary geographically might explain the increase in

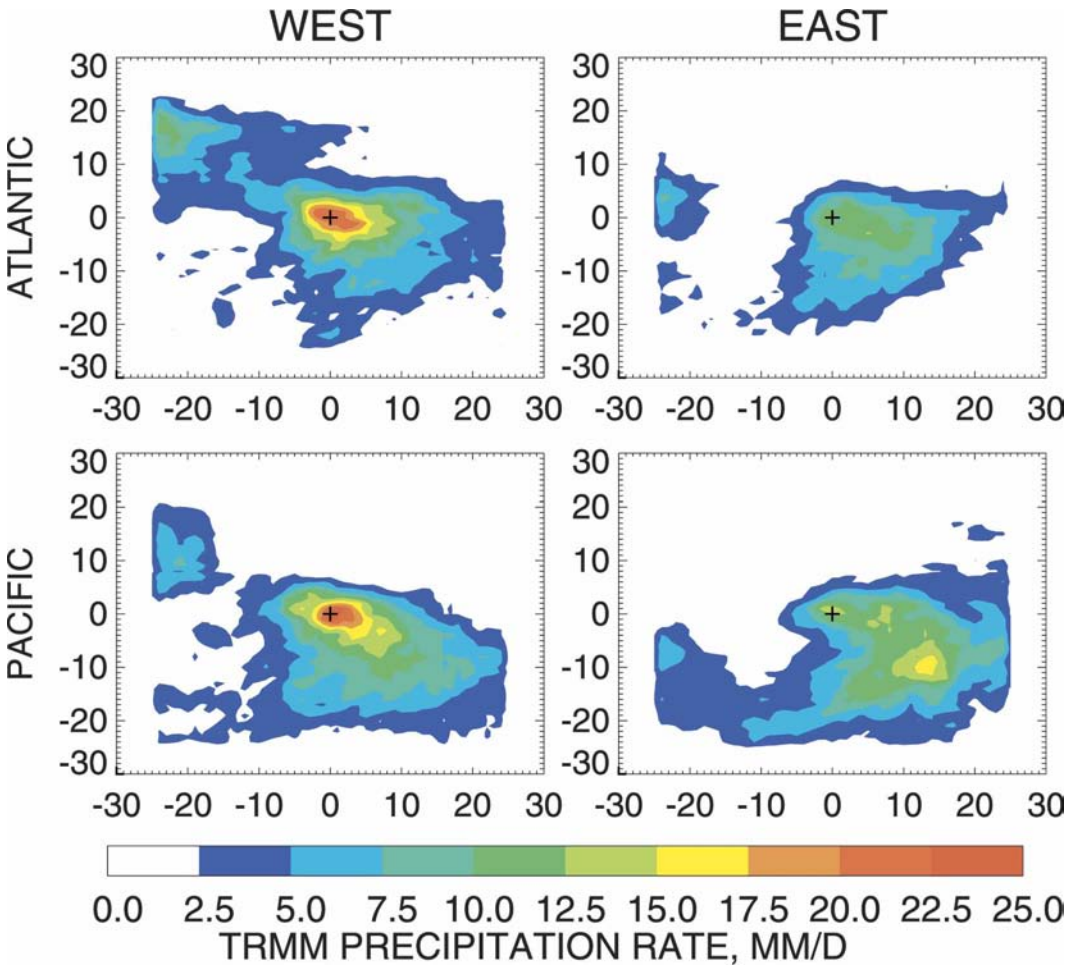

FIG. 9. As in Fig. 8, but for composites of TRMM precipitation rate.

storm cloud-glaciation temperature from west to east. To diagnose whether this might be a signature of the storm life cycle instead, with glaciation becoming more widespread in the mature stage, we produced composites of T_{50} for the initial detection, peak sea level pressure tendency, peak intensity (minimum central pressure), and final detection of all storms, regardless of where these occurred geographically. We found no systematic changes from one life cycle phase to another despite the fact that storm vertical velocities and precipitation are strongest at storm onset and weaken systematically thereafter.

We also looked at possible variations in storm depth (i.e., whether ascent to higher altitude in the frontal zone might affect the cloud-top temperature dependence of glaciation there). However, the composite cloud-top temperature for all clouds (not just those for which ice occurs 50% of the time) is similar in the frontal regions for the western and eastern segments of both ocean basins (Fig. 12). Thus, systematic variations in frontal cloud thickness do not seem to exist.

Aerosols might also produce geographic differences in glaciation since the western oceans downwind of Asian and North American pollution sources have higher aerosol loads than the eastern oceans, the west Pacific more so than the west Atlantic. Mean column aerosol optical depth (observed by MODIS only under clear rather than stormy conditions) is greatest in the southwest sectors of the storm composites, but cloud liquid droplet effective radii retrieved with MODIS (not shown) do not appear systematically different there than elsewhere. This does not rule out the possibility of an aerosol effect on nucleation at higher altitude, but neither is there evidence to suggest that it is a first-order influence.

Thus, we suggest the following picture of processes regulating cloud-top phase as being most consistent with the various composites. In the frontal ascent re-

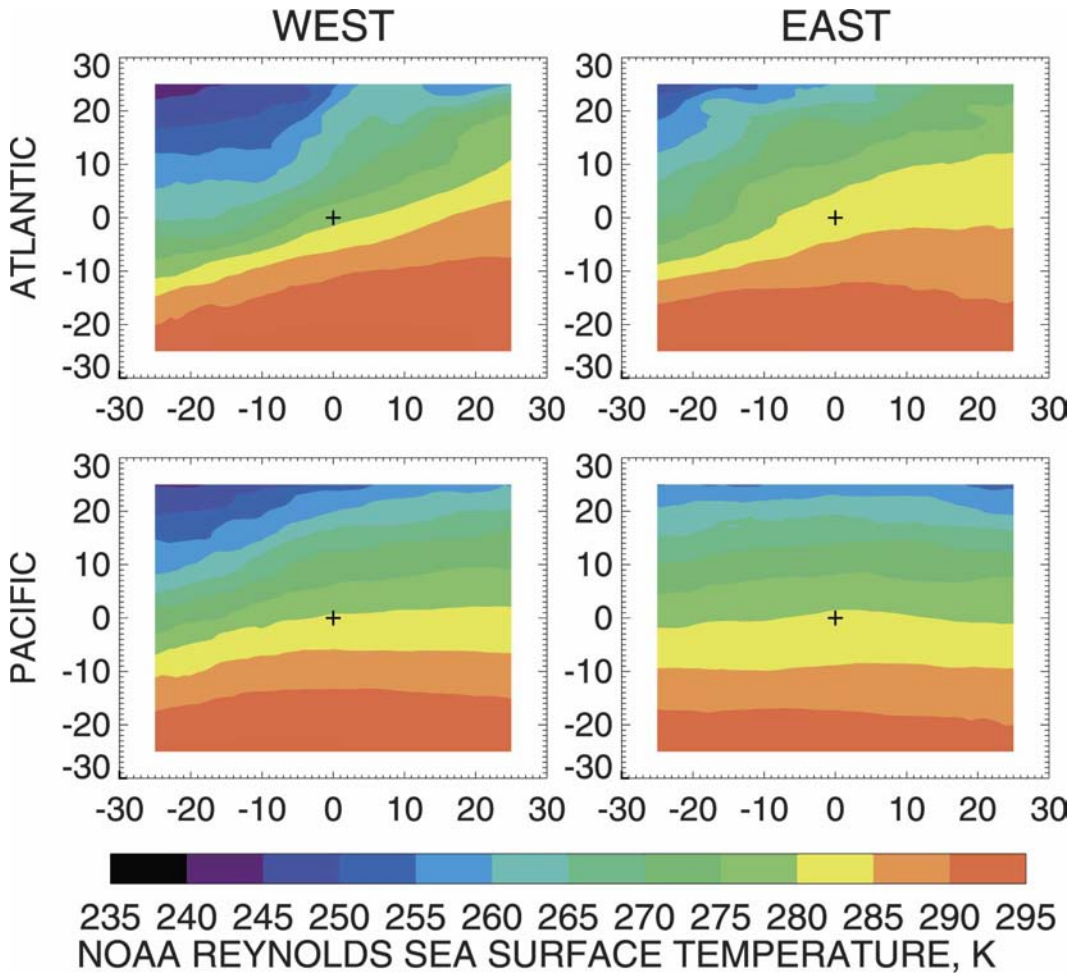

FIG. 10. As in Fig. 8, but for composites of NOAA Reynolds SST.

gion of the storm, where the strongest precipitation rates and highest cloud tops occur, glaciation occurs on average at the warmest temperatures. Cloud tops in these regions are at mean temperatures of ~225–240 K (Fig. 12), where homogeneous nucleation of the ice phase is common and thus ice exists regardless of the ice nucleus concentration. Thus, we only expect MODIS to detect liquid at times and places where cloud top is lower and warmer than the mean value (cf. the region just east of the surface low in Fig. 3). However, the very warm T_{50} values in the frontal region suggest other means of glaciating cloud there, for example, the Bergeron–Findeisen growth of ice crystals at the expense of supercooled water droplets (e.g., Pruppacher and Klett, 1978). The significant pixel-level phase variability that we sometimes see in frontal zones (Fig. 3), the ascent that maintains conditions near water saturation, and T_{50} values close to those at which the Bergeron–Findeisen process operates most efficiently may indicate the presence of such processes limiting liquid occurrence at colder temperatures.

However, T_{50} (Fig. 11) is not warm everywhere that the mean cloud-top temperature is coldest (Fig. 12), for example, in the wraparound region north of the surface low and even in the frontal zone of the west Atlantic. In these locations supercooled droplets apparently do not glaciate as readily and, instead, get lifted to colder temperatures. One possible explanation is the decrease in strength of 500-mb ascent (Fig. 8) from west to east as the SST gradient weakens. Perhaps sufficiently vigorous ascent either suppresses ice formation or advects supercooled liquid water to colder cloud-top levels. Bower et al. (1996) suggest that vigorous updrafts in convective clouds do not leave enough time for supercooled droplets to transform into ice crystals in the Hallett–Mossop zone of ice multiplication by graupel–supercooled droplet collisions at warm temperatures (~267 K). On the contrary, they find larger ice fractions

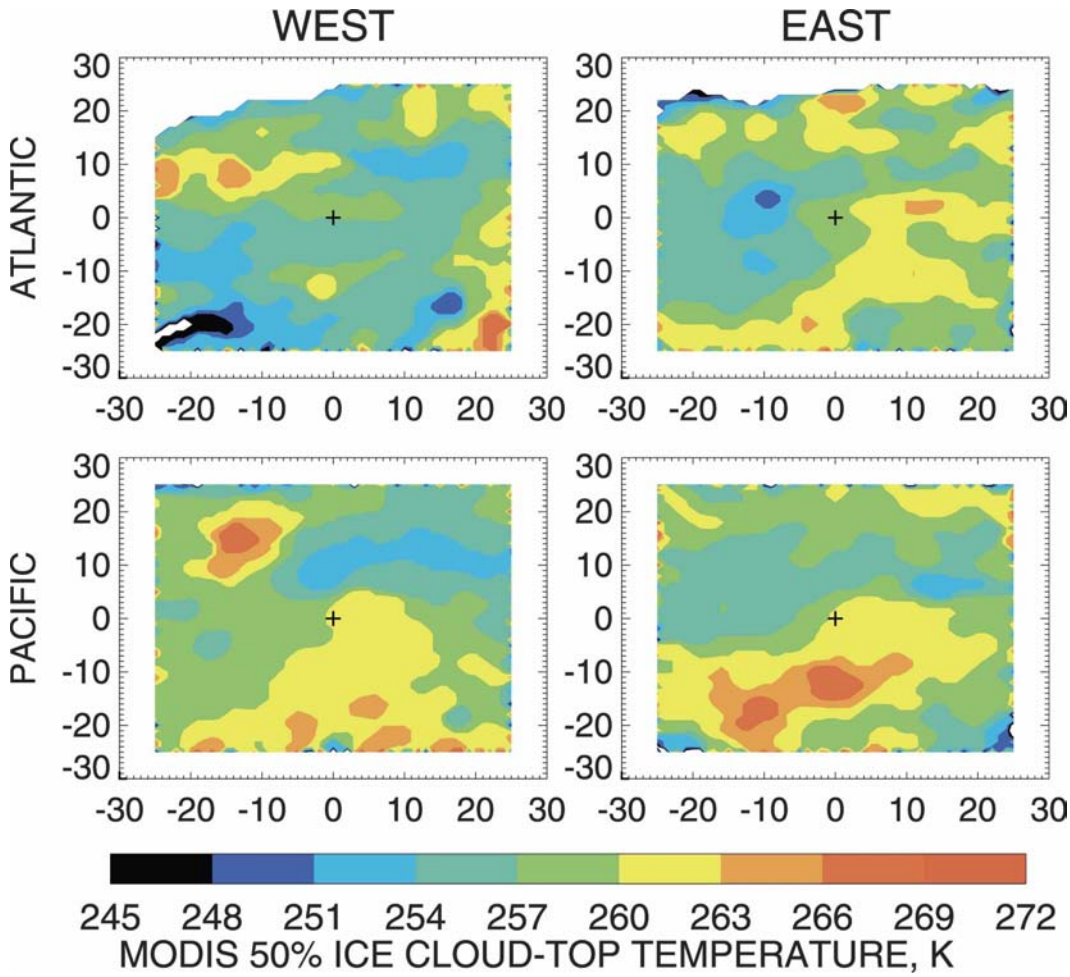

FIG. 11. As in Fig. 8, but for composites of MODIS T_{50}.

in stratiform frontal clouds observed around the British Isles where ascent is weaker. Even in the strongest ascent region of our western ocean storms, mean vertical velocities are only ~15 hPa h^{-1} (~6 cm s^{-1}), well short of typical ice particle fall speeds. However, the strongest ascent regions of storms are the most likely to contain embedded convection, and in a few small-scale regions updrafts may be strong enough to advect supercooled liquid droplets to cloud top where MODIS detects them. Figure 11 therefore suggests the possibility that the Bower et al. frontal data may be more characteristic of weak storms than intense storms if the east–west differences we observe are indicative of similar differences at deeper levels.

By contrast, outside the frontal zones in both ocean basins, glaciation occurs at consistently colder temperatures at cloud top. Mean cloud tops are warmer (i.e., lower) and precipitation weak in these locations, suggesting a preponderance of shallower midlevel altostratus and altocumulus clouds (cf. Lau and Crane 1995), and vertical velocities are weak or even downward. Thus, the odds of sufficient lifting taking place for glaciation to occur are reduced. Bower et al. sampled a few such shallow clouds, but perhaps not a sufficient number to be climatologically representative.

Our results help place previous observations of the cloud liquid–ice transition into a large-scale dynamical context. Doutriaux-Boucher and Quaas (2004) use the formalism of Le Treut and Li (1991) to fit free parameters describing the temperature dependence of thermodynamic phase to satellite polarimetry data:

$$f_{\mathrm{liq}} = [(T - T_{\mathrm{ice}})/(T_{\mathrm{o}} - T_{\mathrm{ice}})]^{n}, \qquad (1)$$

where f_{liq} is the liquid fraction, T the temperature, T_{o} the temperature above which all clouds are liquid, T_{ice} the temperature below which all clouds are ice, and n is a shape parameter that controls the slope of $f_{\mathrm{liq}}(T)$ at intermediate temperatures. Our MODIS-derived parameter T_{50} can be expressed in this formalism as

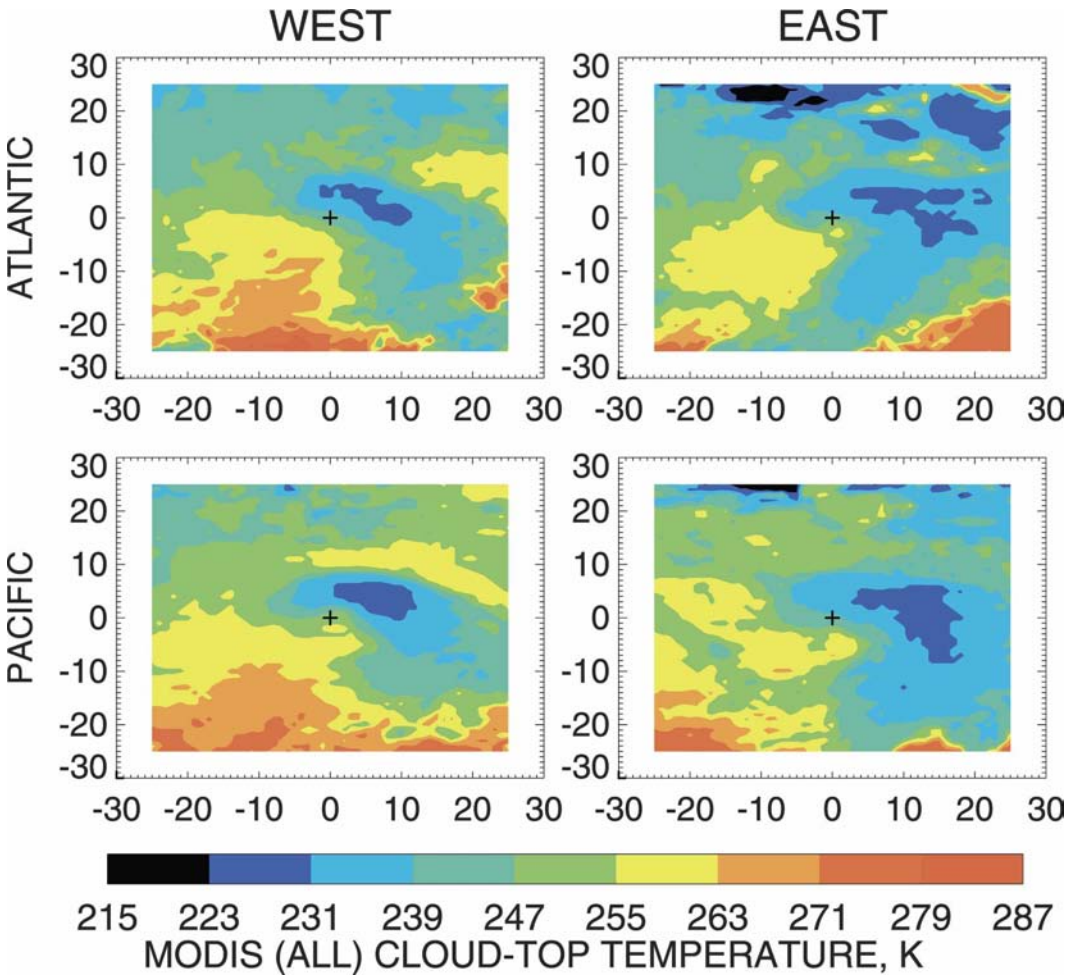

FIG. 12. As in Fig. 8, but for composites of MODIS cloud-top temperature (for all clouds).

$$T_{50} = T_{\text{ice}} + 0.5^{1/n}(T_{\text{o}} - T_{\text{ice}}). \quad (2)$$

For the data they analyze, Doutriaux-Boucher and Quaas assume $T_{\text{o}} = 0°\text{C}$ and find a best fit for $T_{\text{ice}} = -32°\text{C}$ and $n = 1.7$. Using (2), this corresponds to $T_{50} \sim -11°\text{C} \sim 262$ K, somewhat warmer than our mean value for the two ocean basins of ~258 K in the MODIS data. A colder value of $T_{\text{ice}} = -38°\text{C}$, especially if combined with a slightly colder assumed $T_{\text{o}} = -4°\text{C}$ (cf. Del Genio et al. 1996), yields $T_{50} \sim -15°\text{C} \sim 258$ K for the same n, in agreement with our mean value. Aside from retrieval uncertainties in both datasets, the difference may be due to our focus on midlatitude ocean clouds and the fact that the phase retrieval algorithm in the polarization data is applied only to ~60 km × 60 km overcast regions, which may bias that result toward thicker, more extensive cloud decks.

The temperature dependence of f_{liq} in the field experiment data of Bower et al. (1996) is similar to the composite T_{50} values that we infer in the frontal regions of east Atlantic synoptic storms, even though the two datasets apply to different parts of the cloud. However, T_{50} is colder in stratiform clouds outside the frontal region (Fig. 11) and, in general, on the west/north sides of the ocean basins (Fig. 6), regions not sampled adequately or at all by Bower et al. Whether the differences we see at cloud top imply similar differences in the interior of clouds is not known, although in a model it would be possible to determine whether cloud phase relationships near cloud top and within clouds were systematically different.

These results have implications for predictions of cloud feedback and global climate sensitivity since cloud–radiation interactions are most sensitive to properties near cloud top. Models based on Bower et al. (1996) that do not predict the presence of liquid for $T < -15°\text{C}$ may be somewhat biased toward low sensitivity (depending on the degree of difference in param-

eterized microphysical and radiative properties for liquid versus ice) because any cloud increase with warming in the mixed-phase zone will overestimate the negative shortwave feedback and underestimate the positive longwave feedback. This was the issue originally raised by Li and Le Treut's (1992) sensitivity tests. Our results do not directly address the ice – liquid lifetime difference that causes the predicted cloud increase in the models, but any difference between the lifetimes of ice and liquid clouds is reflected indirectly in our occurrence statistics. Thus, parameterizations that misrepresent the processes that control cloud lifetimes should also produce biased ice–liquid occurrence statistics when aggregated over time.

The real message of our study, though, is the need for more physically based approaches to cloud phase parameterization that allow for different phase behavior in different dynamical settings. The GISS GCM parameterization (Del Genio et al. 1996), for example, allows either ice or liquid to exist in a grid box at a given time step. It assumes ice probability at cloud initiation to increase with decreasing T down to $-40°C$, with saturation relative to the liquid phase in the cloudy part of the box being required to form either phase at these temperatures. However, it takes the additional step of allowing supercooled liquid water that forms to subsequently glaciate if sufficient ice precipitation into a lower supercooled liquid layer occurs. The probability of such glaciation is parameterized to peak at temperatures where Bergeron–Findeisen growth is most efficient. Once the ice phase forms, it remains ice unless particles sediment below the melting level. This should allow for higher T_{50} values in frontal regions, as seen in the MODIS data. In fact, the GISS scheme produces $T_{50} \approx 257$ K over ocean for regions in which the Bergeron–Findeisen process is absent and $T_{50} \approx 264$ K averaged over all ocean regions—in the right direction for synoptic effects but overall somewhat warmer than observed.

More recent cloud parameterizations make no direct assumption about cloud phase, instead carrying ice and liquid water as separate prognostic variables and using microphysical process parameterizations to predict statistics of phase–temperature behavior (cf. Lohmann and Roeckner 1996; Wilson and Ballard 1999; Rotstayn et al. 2000). These schemes are potentially a step forward, but they too have free parameters (e.g., ice nucleus concentration), ambiguity about the spatial relationship between liquid and ice within a grid box, and uncertainty in how to scale process rates known on the cloud scale to the GCM grid scale. To date these schemes have been developed using only isolated case studies or limited regional datasets. Even the larger datasets used by Moss and Johnson (1994) and Hogan et al. (2003b) to evaluate existing schemes are climatologically limited spatially (western Europe) and, for the former, temporally (11 flights). Our results provide a framework for a more climatically meaningful evaluation that will indicate any potential biases contributing to erroneous cloud feedback estimates.

5. Conclusions

The relationship between ice phase fraction and cloud-top temperature obtained from two winters of MODIS retrievals over the North Atlantic and North Pacific midlatitude storm tracks reveals differences between the two oceans and between their western and eastern segments. Glaciation occurs at warmer cloud-top temperatures south and east of the storm pressure minimum in the Atlantic and south of the low in the Pacific. Ice cloud formation in midlatitude storm tracks is related to the storm vertical velocity and precipitation, with the distribution around the storm center seemingly related to the SST pattern. Changes in glaciation temperature from the west to east sides of the ocean basins appear to be related to the SST gradient and its effect on storm strength.

Further work is needed to evaluate this relationship quantitatively, as uncertainties in MODIS retrievals need to be assessed first. A new MODIS data reprocessing is in progress, and the new Collection-5 products should be of better quality as the algorithms for both phase and cloud-top temperature have been significantly improved. Comparisons with more precise satellite-based measurements such as the Cloud-Aerosol Lidar and Infrared Pathfinder Satellite Observation (CALIPSO) lidar will be extremely useful to evaluate the impact of thin cirrus over lower water clouds on the relationship between phase and cloud-top temperature retrievals.

Our results at cloud top are similar to those from previous aircraft observations inside clouds over the British Isles in frontal regions (Bower et al. 1996). They suggested that strong local updrafts in convective regions push moist air to cold temperature levels too quickly for various glaciation processes to occur. Here we find that the areas of greatest large-scale ascent are not glaciated at cloud top as much as areas of moderate ascent, but that thick clouds in general glaciate at warmer temperature than shallower mixed-phase clouds, the latter of which were not adequately sampled by Bower et al. (1996).

In addition, glaciation occurs preferentially in the storm perimeter where the warmest SSTs occur. Consequently, ice phase at cloud top occurs more fre-

quently in the southern part of the Pacific and over the south and east regions of the Atlantic. The differences at cloud top between the four subregions studied here raise the possibility that aircraft observations of the temperature of complete glaciation in frontal zones will be different depending on the location, and thus modeling of the phase change cannot be performed either with a unique temperature threshold for the entire globe or with data from a single region as a validation standard. The extent of condensation and droplet growth as influenced by surface temperature and vertical velocities will have to be taken into account as well. For the midlatitude oceans as a whole, supercooled liquid persists to lower cloud-top temperatures than occur in Bower et al.'s (1996) measurements inside clouds, suggesting a possible negative cloud feedback bias in GCMs whose phase parameterizations rely on those data.

Acknowledgments. The authors thank Jeff Jonas, Bryan Baum, Michael King, and Steven Platnick for helpful discussions and three anonymous reviewers for useful comments. This research was supported by the NASA Radiation Sciences and Precipitation Measurement Missions Programs and the DOE Atmospheric Radiation Measurement Program.

REFERENCES

Bauer, M., and A. D. Del Genio, 2006: Composite analysis of winter cyclones in a GCM: Influence on climatological humidity. *J. Climate,* **19,** 1652–1672.

Boville, B. A., P. J. Rasch, J. J. Hack, and J. R. McCaa, 2006: Representation of clouds and precipitation processes in the Community Atmosphere Model Version 3 (CAM3). *J. Climate,* **19,** 2184–2198.

Bower, K. N., S. J. Moss, D. W. Johnson, T. W. Choularton, J. Latham, P. R. A. Brown, A. M. Blyth, and J. Cardwell, 1996: A parameterization of the ice water content observed in frontal and convective clouds. *Quart. J. Roy. Meteor. Soc.,* **122,** 1815–1844.

Chandler, M., and J. Jonas, cited 1999: Atlas of extratropical storm tracks (1961–1998). Tech. Report, NASA Goddard Institute for Space Studies, New York, NY. [Available online at http://www.giss.nasa.gov/data/stormtracks.]

Chang, E. K. M., and S. Song, 2005: Differences between the seasonal cycles in the distribution of precipitation around cyclones in the western North Pacific and Atlantic. Preprints, *15th Conf. on Atmospheric and Oceanic Fluid Dynamics,* Cambridge, MA, Amer. Meteor. Soc., CD-ROM, P6.2.

——, S. Lee, and K. L. Swanson, 2002: Storm track dynamics. *J. Climate,* **15,** 2163–2183.

Del Genio, A. D., M.-S. Yao, W. Kovari, and K. K.-W. Lo, 1996: A prognostic cloud water parameterization for global climate models. *J. Climate,* **9,** 270–304.

Deng, Y., and M. Mak, 2005: An idealized model study relevant to the dynamics of the midwinter minimum of the Pacific storm track. *J. Atmos. Sci.,* **62,** 1209–1225.

Derber, J. C., D. F. Parrish, and S. J. Lord, 1991: The new global operational analysis system at the National Meteorological Center. *Wea. Forecasting,* **6,** 538–547.

Doutriaux-Boucher, M., and J. Quaas, 2004: Evaluation of cloud thermodynamic phase parameterizations in the LMDZ GCM by using POLDER satellite data. *Geophys. Res. Lett.,* **31,** L06126, doi:10.1029/2003GL019095.

Eichler, T., and R. W. Higgins, 2006: Climatology and ENSO-related variability of North American extratropical cyclone activity. *J. Climate,* **19,** 2076–2093.

Feigelson, E. M., 1978: Preliminary radiation model of a cloudy atmosphere. Part I: Structure of clouds and solar radiation. *Contrib. Atmos. Phys.,* **51,** 203–229.

Frey, R., B. A. Baum, W. P. Menzel, S. A. Ackerman, C. C. Moeller, and J. D. Spinhirne, 1999: A comparison of cloud-top heights computed from airborne lidar and MAS radiance data using CO_2-slicing. *J. Geophys. Res.,* **104** (D20), 24 547–24 555.

Giraud, V., O. Thouron, J. Riedi, and P. Goloub, 2001: Analysis of direct comparison of cloud top temperature and infrared split window signature against independent retrievals of cloud thermodynamic phase. *Geophys. Res. Lett.,* **28,** 983–986.

Hakim, G. J., 2003: Developing wave packets in the North Pacific storm track. *Mon. Wea. Rev.,* **131,** 2824–2837.

Hasumi, H., and S. Emori, Eds., 2004: K-1 coupled model (MIROC) decription. K-1 Tech. Rep. 1, Center for Climate System Research, University of Tokyo, 34 pp.

Hogan, R. J., P. N. Francis, H. Flentje, A. J. Illingworth, M. Quante, and J. Pelon, 2003a: Characteristics of mixed-phase clouds. I: Lidar, radar and aircraft observations from CLARE'98. *Quart. J. Roy. Meteor. Soc.,* **129,** 2089–2116.

——, A. J. Illingworth, E. J. O'Connor, and J. P. V. Poiares Baptista, 2003b: Characteristics of mixed-phase clouds. II: A climatology from ground-based lidar. *Quart. J. Roy. Meteor. Soc.,* **129,** 2117–2134.

——, M. D. Behera, E. J. O'Connor, and A. J. Illingworth, 2004: Estimate of the global distribution of stratiform supercooled liquid water clouds using the LITE lidar. *Geophys. Res. Lett.,* **31,** L05106, doi:10.1029/2003GL018977.

Huffman, G. J., R. F. Adler, E. F. Stocker, D. T. Bolvin, and E. J. Nelkin, 2003: Analysis of TRMM 3-hourly multi-satellite precipitation estimates computed in both real and post-real time. Preprints, *12th Conf. on Satellite Meteorology and Oceanography,* Long Beach, CA, Amer. Meteor. Soc., CD-ROM, P4.11.

Kalnay, E., and Coauthors, 1996: The NCEP/NCAR 40-Year Reanalysis Project. *Bull. Amer. Meteor. Soc.,* **77,** 437–471.

Kiehl, J. T., J. J. Hack, G. B. Bonan, B. A. Boville, D. L. Williamson, and P. J. Rasch, 1998: The National Center for Atmospheric Research Community Climate Model: CCM3. *J. Climate,* **11,** 1131–1149.

King, M. D., and Coauthors, 2003: Cloud, aerosol and water vapor properties from MODIS. *IEEE Trans. Geosci. Remote Sens.,* **41,** 442–458.

Kistler, R., and Coauthors, 2001: The NCEP–NCAR 50-year reanalysis: Monthly means CD-ROM and documentation. *Bull. Amer. Meteor. Soc.,* **82,** 247–267.

Klein, S. A., and C. Jakob, 1999: Validation and sensitivities of frontal clouds simulated by the ECMWF model. *Mon. Wea. Rev.,* **127,** 2514–2531.

Lau, N.-C., and M. W. Crane, 1995: A satellite view of the synoptic-scale organization of cloud properties in midlatitude

and tropical circulation systems. *Mon. Wea. Rev.,* **123,** 1984–2006.

Le Treut, H., and Z.-X. Li, 1991: Sensitivity of an atmospheric general circulation model to prescribed SST changes: Feedback effect associated with the simulation of cloud optical properties. *Climate Dyn.,* **5,** 175–187.

Li, Z.-X., and H. LeTreut, 1992: Cloud-radiation feedbacks in a general circulation model and their dependence on cloud modeling assumptions. *Climate Dyn.,* **7,** 133–139.

Lohmann, U., and E. Roeckner, 1996: Design and performance of a new cloud microphysics scheme developed for the ECHAM general circulation model. *Climate Dyn.,* **12,** 557–572.

Mace, G. G., Y. Zhang, S. Platnick, M. D. King, P. Minnis, and P. Yang, 2005: Evaluation of cirrus cloud properties derived from MODIS data using cloud properties derived from ground-based observations collected at the ARM SGP site. *J. Appl. Meteor.,* **44,** 221–240.

Menzel, P., B. Baum, K. Strabala, and R. Frey, 2002: Cloud-top properties and cloud phase algorithm theoretical basis document. ATBD_MOD_04, NASA Goddard Space Flight Center, 62 pp. [Available online at http://modis-atmos.gsfc.nasa.gov/MOD06_L2/atbd.html.]

Mitchell, J. F. B., C. A. Senior, and W. J. Ingram, 1989: CO_2 and climate—A missing feedback. *Nature,* **341,** 132–134.

Moss, S. J., and D. W. Johnson, 1994: Aircraft measurements to validate and improve numerical model parameterizations of ice to water ratios in clouds. *Atmos. Res.,* **34,** 1–25.

Nakamura, H., 1992: Midwinter suppression of baroclinic wave activity in the Pacific. *J. Atmos. Sci.,* **49,** 1629–1642.

Naud, C., J.-P. Muller, and E. E. Clothiaux, 2002: Comparison of cloud top heights derived from MISR stereo and MODIS CO_2-slicing. *Geophys. Res. Lett.,* **29,** 1795, doi:10.1029/2002GL015460.

——, ——, M. Haeffelin, Y. Morille, and A. Delaval, 2004: Assessment of MISR and MODIS cloud top heights through inter-comparison with a back-scattering lidar at SIRTA. *Geophys. Res. Lett.,* **31,** L04114, doi:10.1029/2003GL018976.

——, ——, E. E. Clothiaux, B. A. Baum, and W. P. Menzel, 2005a: Intercomparison of multiple years of MODIS, MISR and radar cloud-top heights. *Ann. Geophys.,* **23,** 2415–2424.

——, ——, and P. de Valk, 2005b: On the use of ICESat-GLAS measurements for MODIS and SEVIRI cloud-top height accuracy assessment. *Geophys. Res. Lett.,* **32,** L19815, doi:10.1029/2005GL023275.

Orlanski, I., 2005: A new look at the Pacific storm track variability: Sensitivity to tropical SSTs and to upstream seeding. *J. Atmos. Sci.,* **62,** 1367–1390.

Platnick, S., M. D. King, S. A. Ackerman, W. P. Menzel, B. A. Baum, J. C. Riédi, and R. A. Frey, 2003: The MODIS cloud products: Algorithms and examples from *Terra*. *IEEE Trans. Geosci. Remote Sens.,* **41,** 459–473.

Pruppacher, H. R., and J. D. Klett, 1978: *Microphysics of Clouds and Precipitation*. 1st ed. Kluwer Academic, 714 pp.

Rauber, R. M., and A. Tokay, 1991: An explanation for the existence of supercooled water at the top of cold clouds. *J. Atmos. Sci.,* **48,** 1005–1023.

Reynolds, R. W., and T. M. Smith, 1994: Improved global sea surface temperature analyses using optimum interpolation. *J. Climate,* **7,** 929–948.

Rotstayn, L. D., B. F. Ryan, and J. J. Katzfey, 2000: A scheme for calculation of the liquid fraction in mixed-phase stratiform clouds in large scale models. *Mon. Wea. Rev.,* **128,** 1070–1088.

Salomonson, V. V., W. L. Barnes, P. W. Maymon, H. E. Montgomery, and H. Ostrow, 1989: MODIS: Advanced facility instrument for studies of the earth as a system. *IEEE Trans. Geosci. Remote Sens.,* **27,** 145–153.

Senior, C. A., and J. F. B. Mitchell, 1993: Carbon dioxide and climate: The impact of cloud parameterization. *J. Climate,* **6,** 393–418.

Wilson, D. R., and S. P. Ballard, 1999: A microphysically based precipitation scheme for the UK Meteorological Office Unified Model. *Quart. J. Roy. Meteor. Soc.,* **125,** 1607–1636.